Analyst

Coordinated Mapping of Li^+ Flux and Electron Transfer Reactivity during Solid-Electrolyte Interphase Formation at a Graphene Electrode

Journal:	*Analyst*
Manuscript ID	AN-ART-12-2019-002637.R1
Article Type:	Paper
Date Submitted by the Author:	18-Feb-2020
Complete List of Authors:	Gossage, Zachary; University of Illinois at Urbana-Champaign, Chemistry Hui, Jingshu; University of Illinois at Urbana-Champaign, Department of Chemistry Sarbapalli, Dipobrato; University of Illinois at Urbana-Champaign, Chemistry Rodriguez-Lopez, Joaquin; University of Illinois at Urbana-Champaign, Chemistry

ARTICLE

Coordinated Mapping of Li^+ Flux and Electron Transfer Reactivity during Solid-Electrolyte Interphase Formation at a Graphene Electrode

Received 00th January 20xx,
Accepted 00th January 20xx

DOI: 10.1039/x0xx00000x

Zachary T. Gossage, Jingshu Hui, Dipobrato Sarbapalli and Joaquín Rodríguez-López*

Interphases formed at battery electrodes are key to enabling energy dense charge storage by acting as protection layers and gatekeeping ion flux into and out of the electrodes. However, our current understanding of these structures and how to control their properties is still limited due to their heterogenous structure, dynamic nature, and lack of analytical techniques to probe their electronic and ionic properties *in situ*. In this study, we used a multi-functional scanning electrochemical microscopy (SECM) technique based on an amperometric ion-selective mercury disc-well (HgDW) probe for spatially-resolving changes in interfacial Li^+ during solid electrolyte interphase (SEI) formation and for tracking its relationship to the electronic passivation of the interphase. We focused on multi-layer graphene (MLG) as a model graphitic system and developed a method for ion-flux mapping based on pulsing the substrate at multiple potentials with distinct behavior (e.g. insertion-deinsertion). By using a pulsed protocol, we captured the localized uptake of Li^+ at the forming SEI and during intercalation, creating activity maps along the edge of the MLG electrode. On the other hand, a redox probe showed passivation by the interphase at the same locations, thus enabling correlations between ion and electron transfer. Our analytical method provided direct insight into the interphase formation process and could be used for evalauting dynamic interfacial phenomena and improving future energy storage technologies.

Introduction

Elucidating the evolution of battery interphases during operation is a major research priority for improving energy storage technologies.[1-7] Achieving high energy densities, as in lithium-ion batteries (LIB) and many next generation technologies, requires redox reactions at very high and low potentials.[1, 4, 8] Consequently, these potentials lead to electrolyte decomposition, forming interphases at the electrodes that regulate electrode reactivity upon further cycling.[1, 4] At negative electrodes, such as a graphitic carbon or Si, the formed interphase is referred to as the solid-electrolyte interphase (SEI) and forms rapidly during the initial cycles.[1, 4] Recent reports using *operando* and *in situ* characterization techniques indicated the SEI structure is morphologically and chemically heterogeneous and continues fluctuating during extended cycling or at open circuit potentials (OCP).[1, 9-14] These characterization techniques have led to improved understanding of the SEI components and precursors, but few works have focused on acquiring information regarding interfacial alkali ion (e.g. Li^+) dynamics during SEI initiation and stabilization in spite of the key role of Li^+ in the energy storage mechanism.[15-17]

Emerging scanning probe methods (SPMs), such as scanning electrochemical microscopy (SECM),[15, 16, 18-20] scanning ion-conductance microscopy (SICM),[21-23] or scanning electrochemical cell microscopy (SECCM),[24, 25] show promise for tracking and understanding interfacial ion dynamics at functional electrodes.[2, 26, 27] Recently, our lab introduced Hg probes and methods combined with SECM to provide localized insight of ion flux within real battery environments.[18, 28] Our group applied these probes to measure ion intercalation[16, 19] and kinetics[15] on graphitic carbons. Also, these probes can utilize the ions to resolve topographical features for both imaging and positioning.[28-30] In few studies, Hg probes were successful at capturing ionic flux images at reacting surfaces.[18, 19, 31] Ionic imaging is a powerful tool for evaluating battery materials and their interphases, providing access to wide temporal and spatial information.[28]

Hg-based SECM probes are easy to prepare and provide the unique opportunity to quantify both ionic and electronic information at the same location.[28] As with other SECM studies, adding a dilute redox mediator to the electrolyte enables evaluation of electron transfer across the passivating SEI.[14, 32, 33] Thereafter, the Hg probe can reversibly switch between feedback or ionic imaging modes through either redox reactions with a mediator or amalgamation/stripping, respectively.[28] This multi-functional probe would help understand how electron and ion transfer reactivity are related, with the ultimate goal of improving interphase stability and function.[2, 34]

Department of Chemistry, University of Illinois at Urbana-Champaign, 600 S Mathews Ave., Urbana, Illinois 61801, United States.
**To whom all correspondence should be addressed: Prof. Rodríguez-López: joaquinr@illinois.edu (Email) and 217-300-7354 (Phone).*
†Electronic Supplementary Information (ESI) available: COMSOL simulations, and additional experimental data. See DOI: 10.1039/x0xx00000x

In this work, we take advantage of the multimodal nature of the Hg probe for extracting and comparing electron and ion transfer at operating multi-layer graphene (MLG) electrodes. We chose MLG as a model graphitic electrode because previous studies on MLG showed fast rate capabilities for (de)intercalation and extensive SEI formation.[19, 35, 36] Using mercury disc-well (HgDW) microelectrodes,[28] we tracked Li^+ dynamics at different locations during SEI formation and (de)intercalation processes. With the redox mediator couple, *N,N,N′,N′*-tetramethyl-*p*-phenylenediamine (TMPD/$TMPD^+$), we positioned the probe near the thin MLG surface and coordinated Li^+ flux measurements with the MLG potential and electron transfer across its surface throughout the experiments. We introduced a pulsed mapping procedure based on cyclic voltammetry SECM (CV-SECM)[19, 28, 29] to minimize bulk substrate effects and more effectively measure localized Li^+ flux. We discuss the impact of the extended electrode surface on Li^+ flux maps and the invaluable insight that is accessible through our approach and for future *in situ* studies.

Experimental

Materials and methods

For the Li^+ source, we used lithium hexafluorophosphate ($LiPF_6$, ≥99.99%) and lithium tetrafluoroborate ($LiBF_4$, ≥99.99%) from Sigma Aldrich. Also, tetrabutyl ammonium hexafluorophosphate ($TBAPF_6$ (Sigma Aldrich, 99%)) acted as an additional supporting electrolyte. *N,N,N′,N′*-tetramethyl-*p*-phenylenediamine (TMPD, 99%, Sigma Aldrich) was used as the redox mediator. All electrolyte solutions were prepared in 1:1 (by volume) propylene carbonate (PC, anhydrous, 99.7%, Sigma Aldrich) and ethylene carbonate (EC, anhydrous, 99%, Sigma Aldrich). Platinum ultramicroelectrodes (Goodfellow, purity 99.9%, 12.5 µm radius) were prepared as described previously.[28, 37] All purchased chemicals were used as received without further purification.

Substrate preparation and characterization

Multilayer graphene samples were grown and transferred as described previously.[35] The MLG samples were heterogenous and consisted of several graphene layers, with the thickest regions at ~20 layers and thinnest regions below 5 layers.[35] In brief, MLG was grown by chemical vapor deposition (CVD) using methane and 25 µm Cu foil as catalyst. The graphene was transferred onto SiO_2/Si wafers through a wet transfer method as described previously.[19] Fully transferred samples were then patterned using tweezers or tape. Substrates were imaged using scanning electron microscopy (Hitachi S-4700).

HgDW preparation and characterization

HgDW probes were prepared as previously described.[28] In brief, Pt ultramicroelectrodes (UME) were etched for 2-15 s in saturated $CaCl_2$, 1% HCl using a 60 Hz AC-waveform with a peak-to-peak amplitude of 2.7 V. Thereafter, the etched UMEs were submerged in a $Hg(NO_3)_2$ solution (~10 mM) with KNO_3 supporting electrolyte. We used a Ag/AgCl reference and a tungsten wire counter electrode. The probe was poised to reduce and deposit Hg to slightly overfill the etched cavity, as confirmed via optical microscopy. Finally, a coverslip was used to press and flatten the Hg droplet into a disc.[28] We also used voltammetry to characterize the probe before/after etching and pressing.

Scanning Electrochemical Microscopy and Flux Measurements

All electrochemical measurements were performed using a CHI920D Scanning Electrochemical Microscope (CH Instruments, Inc.) inside an oxygen and moisture-free glovebox (maintained at or below 0.1 ppm). The SECM was placed on a BM-10 Vibration Isolation Platform (Minus K). The MLG substrates were assembled in a standard SECM cell, transferred into the glovebox and rinsed three times with PC before SECM experiments. Thereafter, we replaced the PC with other electrolytes as indicated in the text. We leveled and imaged the substrate using a Pt UME of 12.5 µm radius, with a Pt wire as the counter electrode and a clean Li strip as the reference.

For Li^+ flux measurements, we replaced the SECM probe with a HgDW. We refilled the cell with ~2 mM TMPD, 10 mM $LiPF_6$ and 100 mM $TBAPF_6$ and repositioned the HgDW near the MLG substrate. We collected voltammetry at the HgDW with cyclic voltammetry to quantify Li^+ flux change in the vicinity of the probe at selected positions on MLG. We applied potential steps to the substrate in 100 mV increments between 2.5 and 0.5 V vs. Li^+/Li to generate the SEI film.

Pulsed CV-SECM

To conduct Li^+ flux imaging, we took two approaches: 1) *in situ* formation of the SEI in the presence of TMPD and subsequent ionic mapping; or 2) preforming the SEI in a Li^+ electrolyte without TMPD. For the 1st approach, we again positioned the HgDW near an MLG substrate using TMPD. Thereafter, the HgDW was cycled while pulsing the MLG substrate to form the SEI or for (de)intercalation at different potentials; typically alternating the potential of the MLG substrate between anodic (more positive) and cathodic (more negative) potentials. After pulsing the MLG at each potential, the probe was rastered across its surface in 10 µm steps. The stripping peak current, i_{sp}, and integrated substrate charge were extracted for interpreting the results and developing the ionic flux maps.

For the 2nd approach, we preformed the SEI before flux measurements. First, we collected a feedback image using a Pt UME and TMPD; then rinsed the cell thoroughly. Next, we formed the SEI layer on MLG by cycling in 0.1 M $LiBF_4$ electrolyte using recently developed procedures to generate an SEI with full coverage over the substrate, conducive to clear intercalation behavior.[35] After observing reproducible (de)intercalation peaks, we replaced the solution with 5 mM TMPD, 10 mM $LiBF_4$, and 500 mM $TBAPF_6$ in PC:EC. We replaced the Pt UME with a HgDW and positioned the probe for pulsed CV-SECM imaging of the (de)intercalation process. While pulsing the SEI-covered MLG, we used single voltammograms at the HgDW with a 3 s wait time between MLG potential steps. After each potential was measured, the probe was again moved

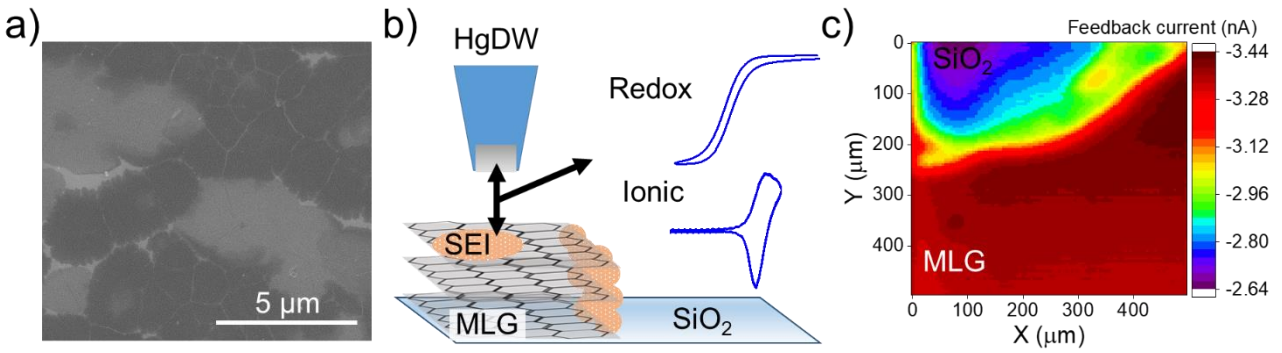

Figure 1. Analysis of MLG using multimodal probes with SECM. a) SEM micrograph of a fresh MLG substrate. b) Illustration of multimoda measurements using the HgDW, with steady-state amperometry using a redox mediator to image the substrate via feedback mode SECM and CV-SECM using the reversible amalgamation of alkali ions for measuring ionic reactivity. c) SECM feedback image of an MLG substrate before SEI formation using 1.5 mM TMPD. The probe was positioned 12 µm above the MLG surface for imaging.

in 10 µm increments across the SEI surface to acquire a profile of changes in Li^+ along MLG.

Results and discussion

Li^+ flux measurement during SEI formation at MLG

First, we focused on evaluating Li^+-based SEI formation at MLG substrates deposited on SiO_2. The MLG films were grown via CVD[19, 35] and showed large micron-sized grains (Figure 1a). By utilizing the redox mediator, TMPD, we positioned the HgDW probes near the reactive MLG for electron transfer and ionic measurements during the SEI formation process (Figure 1b) with the former performed using the redox mediator in the feedback mode, and the latter performed via transient CV-SECM measurements using the reversible amalgamation of Li^+ in Hg. After leveling using a Pt UME, we collected a feedback SECM image of the freshly transferred MLG sample (Figure 1c). In line with previous reports using SECM on graphene-based materials, we observed positive feedback and fast electron

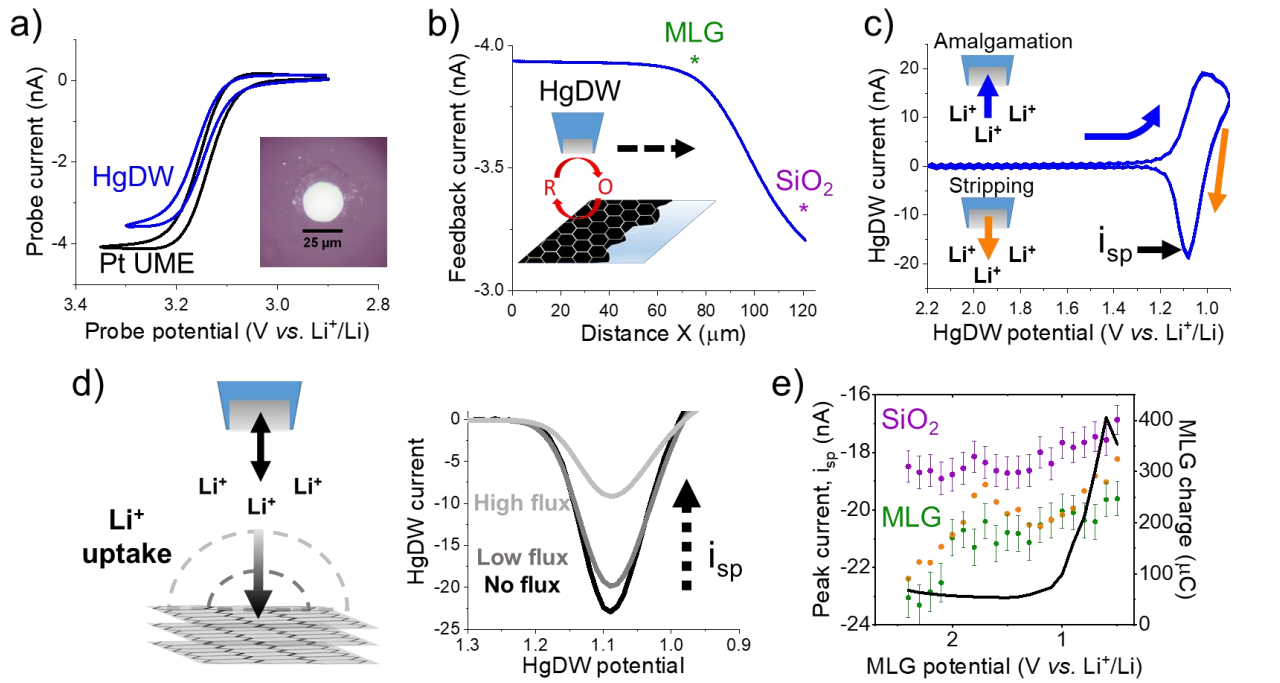

Figure 2. Tracking Li^+ during SEI formation on MLG. a) Comparison of cyclic voltammetry of 2 mM TMPD at a HgDW and Pt UME of the same electrode radius after transfer into a glovebox. The inset shows the pristine HgDW after Hg deposition and pressing. b) Line scan across the MLG and SiO_2 wafer for positioning the HgDW. The probe positions are indicated relative to the MLG surface during two measurements, on separate samples. The inset is an illustration depicting the line scan process for positioning using a redox mediator. c) Amalgamation/stripping voltammetry of Li^+ at the HgDW probe for 5 cycles before initiating SEI formation. The stripping peak current, i_{sp}, is labelled. d) Diagram of competition between the HgDW and an MLG substrate during lithiation and the effect on i_{sp}. e) Extracted i_{sp} and integrated charge at MLG for each potential step during the first SEI cycle with the HgDW positioned above the SiO_2 and MLG. The green curve involves measurements collected 1.5 s after each potential step. The orange curve are collected later at ~11 s. For the probe above SiO_2, we determined a standard deviation of less than ± 1.5% i_{sp} as indicated with the error bars.

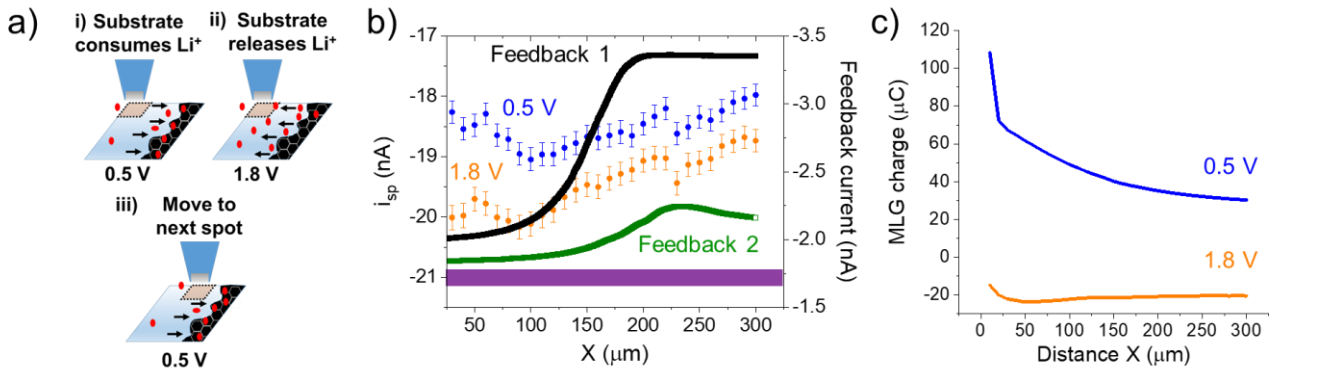

Figure 3. Measuring Li^+ during line scans across MLG while pulsing. a) Illustration of the pulsing methodology for acquiring Li^+ flux maps. b) Measurements of i_{sp} during pulsing while scanning across an MLG substrate during SEI formation. Ionic data overlay feedback measurements using 1.5 mM TMPD before (black) and after the SEI line scan (green). The purple band represents the baseline i_{sp} before polarizing the MLG with its standard deviation of ± 1%. c) Integrated response of the MLG substrate during each pulse.

transfer across all of our MLG samples[19, 38] with some diffusional broadening near uncovered SiO_2 regions at the MLG edge, and clear negative feedback resulting from diffusional blocking of the redox mediator at the SiO_2.

For evaluating ion flux at MLG, we replaced the Pt UME with a HgDW and compared their voltammetry. As seen in Figure 2a, cyclic voltammetry (CV) of TMPD at the HgDW displayed a similar voltammetric response to that of Pt UME, indicating a comparable probe size and geometry. We observed only a slight discrepancy which we attribute to some recessing of the Hg disc caused by transfer into the glove box. After approaching (Figure S1) and positioning the HgDW above the MLG surface (Figure 2b, S2), we cycled the probe for amalgam/stripping of Li^+/Li(Hg), which displayed a consistent signal across multiple cycles (Figure 2c). While continually cycling the HgDW, we biased the MLG electrode to 2.5 V vs. Li^+/Li, then stepped its potential in increments of -100 mV to 0.5 V vs. Li^+/Li with each potential condition held for 12 s. By continually cycling the probe, we could evaluate changes in Li^+ throughout each potential step.

We focused on changes in the stripping peak currents, i_{sp}, to track Li^+ flux occurring near the probe (Figure 2d) during SEI formation and (de)intercalation processes.[15] HgDWs capture Li^+ flux through competition with the substrate (Figure 2d) where a decrease in the absolute value of i_{sp} indicates an influx of Li^+ to the substrate, while an increase above the baseline level indicates outflux.[28, 39] In Figure 2e, we extracted i_{sp} from the HgDW measurements for experiments with the HgDW positioned over SiO_2 and above the MLG. These are plotted alongside the integrated current response, i.e. the charge passed, of one of the MLG samples following our previous analysis.[15] We note the baseline i_{sp} can vary slightly for different probes and positioning. With the HgDW positioned above the MLG, we observed a significant decrease in i_{sp} potentials near 2.1 V, 1.7 V and below 1 V vs. Li^+/Li. As the substrate was biased for longer times, these peaks became more pronounced as shown comparing measurements at 1.5 s (green curve) and 11 s (orange curve) after the start of the potential step. The substrate response for all of our MLG samples showed a cathodic process occurring between 2.3 V and 2.5 V (Figure 2e, Figure S3) related to SEI formation in this potential region.[19, 35]

For the second SEI peak at ~ 1 V on the MLG response (Figure 2e), we again observed a probe response in line with Li^+ consumption by SEI formation. Previous results on MLG and other graphitic systems indicated multiple cathodic peaks between 2.5 V and 0.4 V during SEI formation,[19, 40] though the specific reactions are still unclear.[1]

When sweeping the MLG electrode back positive, the HgDW response did not return to baseline (Figure S4). Consumption of Li^+ from the bulk MLG surface lead to non-localized effects on the tip response[41] likely from a growing concentration gradient near the MLG surface. 2D COMSOL simulations of Li^+ diffusion at this probe-MLG interface agreed that a cathodic pulse at the extended MLG substrate would cause a large decrease in Li^+ and require a significant time (>100 s) to recover back to baseline (Supporting Information, section 2). Therefore, our results indicated an irreversible SEI-formation process at MLG that did not lead to significant Li^+ release.[19, 36] To further verify our measurement, we used another MLG sample and positioned the probe above the SiO_2 (Figure 2b, e). While decreasing the MLG potential, we observed some small change in the i_{sp}; <1.5% standard deviation across the entire potential range, and little difference when comparing measurements at short and long times (Figure S5). Despite the non-localized effects observed at low potentials (<0.7 V vs. Li^+/Li) and accumulated effect from surrounding bulk substrate, our results clearly indicated the sensitivity of the probe toward location-dependent changes of ionic flux as Li^+ was consumed during the SEI formation process.

Coordinating localized electron and Li^+ flux during SEI formation

Next, we explored CV-SECM based imaging[19, 28, 29] to evaluate Li^+ flux during SEI formation at different locations. We now focused on pulsing the potential of the substrate between a condition well into SEI formation (0.5 V vs Li^+/Li) and its reversal to a condition near its onset (1.8 V vs Li^+/Li), as depicted in Figure 3a. This was done to restore the diffusion layer before stepping the probe to a different location. Pulsing the substrate minimizes non-localized effects as applied in redox competition imaging[42] to provide a more stable background and improved mapping.

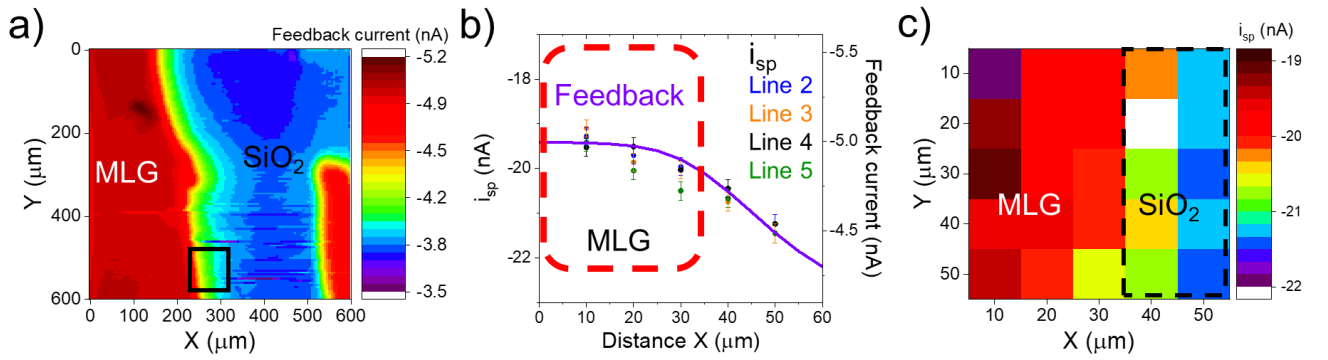

Figure 4. Measuring redox and ion transfer at the peripheries of an MLG surface. a) SECM feedback image before SEI formationusing 2 mM TMPD. The approximate location of interest is shown using the black square. b) Comparison of variation in feedback using TMPD (purple) and i_{sp} while scanning in the X-direction away from the MLG electrode. Feedback current was measured at OCP before forming the SEI. Ion measurements were collected while applying pulses at 1.8 V (anodic) and 0.1 V (cathodic) for (de)intercalation. c) Composite Li^+ flux image from the cathodic pulse (Li^+ uptake) measurements. For every pixel, we applied 2.6 s pulses to the substrate, totalling ~ 6 minutes to collect the flux image.

We first used feedback with a low concentration of TMPD to ease positioning and to coordinate measurement of electron and ion transfer. After positioning the HgDW near an MLG substrate (Figure S6), we collected a line scan of the feedback response (Figure 3b, black curve). After cycling the HgDW toward amalgamation/stripping with Li^+ (Figure S7), we observed <1% standard deviation at the probe across 15 cycles indicating reproducible operation of the probe in the absence of substrate perturbation. We rastered the probe step-wise across the MLG/SiO_2 region while alternating the substrate potential between cathodic pulses at 0.5 V for SEI formation and anodic pulses at 1.8 V (Figure 3b). During initial cathodic pulses, we observed a large Li^+ flux toward the MLG at a lateral distance of ~100 μm from the MLG edge (Figure S8), which we ascribe to substantial SEI formation due to the large potential step and highly reactive, fresh MLG surface (Figure S8). This initial transient subsided after c.a. 3 pulses. As seen in Figure 3b, changes in i_{sp} indicated the formation of a Li^+ concentration gradient that was primarily localized over the MLG surface. In this case, the local concentration of Li^+ was diminished above the active surface during the cathodic and anodic pulses. We note that the Li^+ flux during the cathodic pulse consistently resulted in a larger decrease in i_{sp}, than the anodic pulse, as expected for a higher rate of SEI formation at 0.5 V vs 1.8 V. This result agrees well with the substrate response during the pulse measurements (Figure 3c) suggesting irreversible SEI formation reactions. [19]

After measuring the pulsed ionic flux during SEI formation, we again scanned across the same region using feedback with TMPD (Figure 3b, green curve). The electron transfer rate had significantly decreased from the mass transfer limited value observed before forming the SEI, down to $<10^{-5}$ cm/s.[39, 43, 44] We observed a correlation between the most active regions of the MLG and changes in i_{sp}. At the 100 μm position in Figure 3b, the edge of the Li^+ gradient was well resolved and showed similar broadening to the feedback response. A notable peak in i_{sp} occurred at 225 μm, which is related to a high feedback region and suggesting some Li^+ release during the anodic pulse. Through our methodology, we were able experimentally confirm that most of the MLG surface was undergoing passivation and Li^+ consumption during SEI formation. Few regions showed higher reversibility with outward Li^+ flux during anodic pulsing. These results are in line with previous SECM works suggesting heterogeneities and transient events at the SEI.[14]

2D Li^+ flux maps of (de)intercalation

Next, we expanded our pulsed mapping methodology to 2D scans while focusing on the (de)intercalation process. In this case, we decreased the cathodic pulses to lower intercalation potentials of 0.1 V vs. Li^+/Li for more reversible Li^+ uptake and release.[19] After positioning the probe near the edge of the MLG substrate (Figure 4a, black box), we again formed the SEI using potential steps at the substrate between 2.5 and 0.5 V (Figure S3b). Subsequently, we continued performing line scans with a substrate pulse sequence between 1.8 V and 0.1 V vs. Li^+/Li to drive (de)intercalation. As with the single line scan in Figure 3, we observed a localized decrease in Li^+ near the substrate upon each subsequent line scan (Figure 4b). The diffusional broadening observed in the Li^+ flux measurement was similar to that observed for feedback (Figure 4b). Further, 2D simulations of the probe at different locations with respect to the MLG confirmed this transition from the MLG electrode to its edge and then to the SiO_2 (Supplemental Section 2). Finally, after modifying the Y position, we were able to map the edge of the MLG substrate in a composite SECM image (Figure 4c) within minutes; showing that our pulsed approach successfully captured the active (MLG) and inactive (SiO_2) regions of the substrate as judged by the clear differences in i_{sp} along the X axis.

With this sample, we did not observe substantial Li^+ outflux during anodic pulses (Figure S9), i.e. an enrichment of the local Li^+ concentration reflected in an i_{sp} value larger than the baseline. We posit that our *in situ* procedure did not form a stable SEI capable of reversible (de)intercalation.[19] Alternatively, it is also possible that the Li^+ outflux signal is convolved with residual Li^+ influx to the substrate. To examine

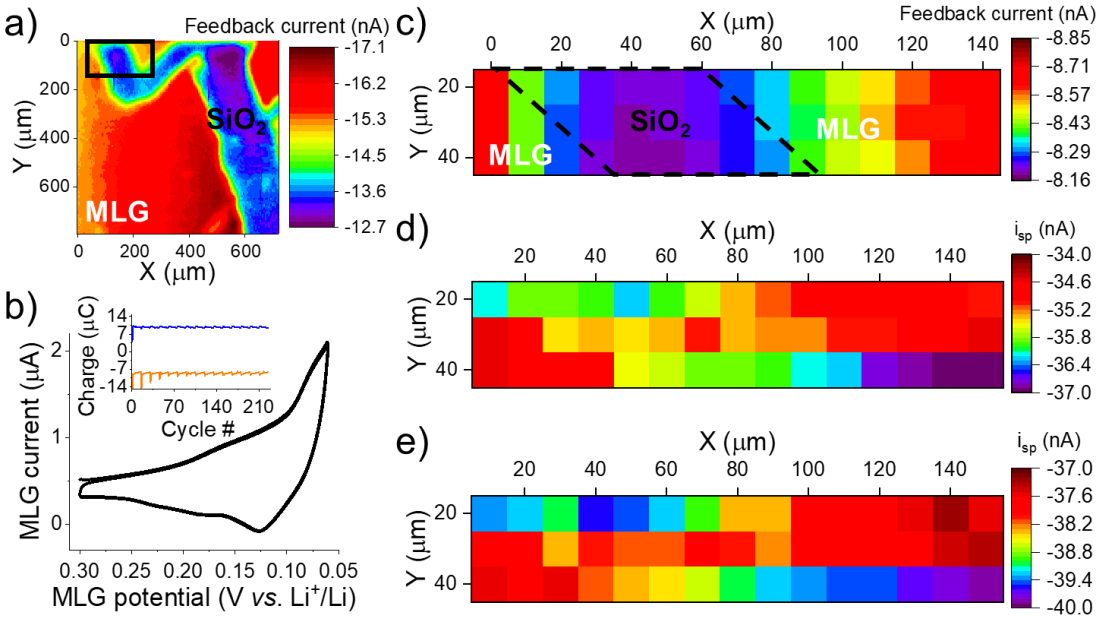

Figure 5. Ionic flux mapping on a preformed SEI. a) Feedback image of a mark on the MLG substrate before SEI formation. A Pt UME was used for imaging in 0.1 M $LiBF_4$, 5 mM TMPD in PC:EC. b) Voltammetry of (de)intercalation after SEI formation in 0.1 M $LiBF_4$. The inset shows the integrated MLG response during pulsed ionic imaging for pulses at 0.06 (blue) and 0.3 V (orange). c) Feedback imaging using 5 mM TMPD across the SEI-covered MLG. d) Li^+ flux image during intercalation pulses at 0.06 V. e) Li^+ flux image during deintercalation pulses at 0.3 V. For every pixel we applied 1.5 s pulses with a 3 s quiet time between each pulse, totalling ~ 20 minutes to collect the flux image.

these possibilities, we turned to an MLG sample with a well-defined intercalation signature by preforming its SEI.

With the preformed SEI, we could confirm the (de)intercalation process and minimize interactions between the redox mediator and the forming SEI. After collecting the SECM feedback image of the MLG substrate (Figure 5a), we retracted the SECM probe, rinsed the cell and replaced the solution with 0.1 M $LiBF_4$ in PC:EC. During an initial negative sweep (Figure S10), we observed several peaks for the SEI formation process in line with previous report.[19] The SEI passivated the substrate substantially during initial sweeps to a capacitive background (Figure S10). Cycling the substrate at more negative potentials (Figure 5b) showed two sets of reproducible peaks for (de)intercalation, agreeing with previous reports on Li^+ (de)intercalation in similar MLG systems.[19, 35, 36]

For conducting pulsed imaging, we replaced the solution with 0.5 M $TBAPF_6$, 10 mM $LiBF_4$ and 5 mM TMPD without rinsing. Using feedback, we approached the HgDW to the MLG substrate and cycled it toward Li^+ amalgamation/stripping (Figure S11). While cycling and moving the probe, we pulsed the substrate to 0.06 then 0.3 V vs. Li^+/Li at each location. Each potential was held for 5 s while measuring with the HgDW leading to a total time of ~20 minutes to collect the two pulse images. The MLG response remained consistent across hundreds of pulses (Figure 5b, inset). We attribute the fluctuations during the initial pulses to restabilization and further formation of the SEI (Figure S12).

We observed good matching between the feedback response (Figure 5c), collected before initiating pulsed imaging, and the pulsed (de)intercalation images (Figure 5d, e) using the same step-size. As seen in Figure 5c, the feedback current indicated negative feedback at the SiO_2 and a mostly passivated SEI-covered MLG displaying some positive feedback. Figure 5d shows that the feedback-active MLG surface induced an inward Li^+ flux while biasing the electrode to 0.06 V. This behavior is expected for the influx of ions caused by intercalation. The subsequent anodic pulses (Figure 5e) showed a higher i_{sp} than the cathodic pulses across the entire surface suggesting Li^+ release by the MLG. This strongly suggests the ability of our probe to detect inward and outward fluxes and to leverage the positioning capabilities of the SECM to map active areas engaged in these processes. This represents an improvement over our recently reported methodology which explored single locations.[15]

Figure 5e again indicated a lower i_{sp} compared to the initial i_{sp} baseline (56 nA, Figure S13). Still, we observed much larger differences between the cathodic and anodic pulses compared with the *in situ* formed SEI (Figure 4c, S9). We believe the probe response at this potential remains affected by some process that continuously consumes Li^+, as we observed previously.[15]The exact cause remains unclear. Additionally, we observed some changes in the background Li^+ level above the insulating region indicating some disturbance from the pulsed protocol. Despite these issues, our approach revealed broad possibilities for understanding ion fluxes near active battery electrode materials. Understanding ionic flux at different times and locations, and further correlating these properties with other relevant battery parameters such as electron transfer, will be key to detangling the complex chemistry occurring during formation and evolution of battery interphases.

Conclusions

In conclusion, we introduced an SECM approach that acquired localized redox and ionic information at an evolving MLG interface used as a Li^+ intercalation electrode. We developed a mapping methodology for Li^+ and redox reactivity by first exploring the use of a pulsing sequence at the substrate coupled to HgDW SECM probe operation and rastering. Our methodology was capable of detecting Li^+ fluxes resulting from SEI formation and intercalation processes with temporal and spatial resolution over various MLG geometries. While forming the SEI with potential steps, we first observed a broad signal indicating Li^+ consumption which was consistent with the irreversible nature of Li^+ uptake while forming the SEI at MLG. By pulsing the substrate during ionic imaging, we observed location-dependent uptake of Li^+ across MLG-SiO_2 surfaces; Li^+ uptake was observed on progressively passivated regions towards electron transfer, confirming the insulating nature of the SEI. Diffusional broadening during Li^+ flux mapping was shown to be consistent with that displayed by feedback measurements, and further confirmed via COMSOL simulations. Upon polarizing the MLG further negative toward (de)intercalation, we observed further SEI formation and location-specific uptake of Li^+ that coordinated well with heterogeneous substrate distribution in feedback mapping. By coordinating potential pulse methods at the substrate with displacements of the SECM probes we gained swift access to exploring both reversible and irreversible processes involving Li^+ fluxes.

We expect that further miniaturization of the probes to sub-micron sizes (50 – 300 nm radius), ongoing in our laboratory, will lead to higher spatial resolution to better match the substrate geometry, e.g. individual grains/domains, particles, etc.[45] Hg probes of smaller electrode size can be prepared,[18] but face their own challenges including saturation of the small Hg volume, droplet loss during handling, and more tedious probe characterization. Along with the developments in this work, unlocking the potential of Hg probes will provide vast opportunities to tackle relationships between interfacial processes and cycling performance in next-generation ion batteries.[46-48]

Conflicts of interest

There are no conflicts to declare.

Acknowledgements

The authors gratefully acknowledge financial support from the National Science Foundation under grant NSF CHE 1709391. Sample preparation and characterization were carried out in part in the Materials Research Laboratory, University of Illinois. Z.T.G. acknowledges the ACS Division of Analytical Chemistry Summer Fellowship and the Hinoree T. and Mrs. Kimiyo Enta Fellowship for support. J.R.-L. acknowledges the Alfred P. Sloan Foundation Fellowship.

Notes and references

1. A. M. Tripathi, W.-N. Su and B. J. Hwang, *Chem. Soc. Rev.*, 2018, **47**, 736-851.
2. J. Hui, Z. T. Gossage, D. Sarbapalli, K. Hernández-Burgos and J. Rodríguez-López, *Anal. Chem.*, 2018, **91**, 60-83.
3. G. Crabtree, G. Rubloff and E. Takeuchi, Basic research needs for next generation electrical energy storage, *Report of the Office of Basic Energy Sciences Workshop on Energy Storage*, U.S. Department of Energy Office of Science, Washington, D.C., 2017.
4. S. K. Heiskanen, J. Kim and B. L. Lucht, *Joule*, 2019, **3**, 2322-2333.
5. M. Ahmed, A. Z. Yazdi, A. Mitha and P. Chen, *ACS Appl. Mater. Interfaces*, 2018, **10**, 30348-30356.
6. R. Zhao, S. Bobev, L. Krishna, T. Yang, J. M. Weller, H. Jing and C. K. Chan, *ACS Appl. Mater. Interfaces*, 2017, **9**, 41246-41257.
7. D. X. Liu, J. Wang, K. Pan, J. Qiu, M. Canova, L. R. Cao and A. C. Co, *Angew. Chem. Int. Ed.*, 2014, **53**, 9498-9502.
8. R. Fong, U. Von Sacken and J. R. Dahn, *J. Electrochem. Soc.*, 1990, **137**, 2009-2013.
9. J. Nanda, G. Yang, T. Hou, D. N. Voylov, X. Li, R. E. Ruther, M. Naguib, K. Persson, G. M. Veith and A. P. Sokolov, *Joule*, 2019, **3**, 2001-2019.
10. C. Cao, I. I. Abate, E. Sivonxay, B. Shyam, C. Jia, B. Moritz, T. P. Devereaux, K. A. Persson, H.-G. Steinrück and M. F. Toney, *Joule*, 2019, **3**, 762-781.
11. H.-Y. Song and S.-K. Jeong, *J. Power Sources*, 2018, **373**, 110-118.
12. L. Seidl, S. Martens, J. Ma, U. Stimming and O. Schneider, *Nanoscale*, 2016, **8**, 14004-14014.
13. D. Lu, J. Tao, P. Yan, W. A. Henderson, Q. Li, Y. Shao, M. L. Helm, O. Borodin, G. L. Graff and B. Polzin, *Nano Lett.*, 2017, **17**, 1602-1609.
14. H. Bülter, P. Schwager, D. Fenske and G. Wittstock, *Electrochim. Acta*, 2016, **199**, 366-379.
15. Z. T. Gossage, J. Hui, Y. Zeng, H. Flores-Zuleta and J. Rodríguez-López, *Chem. Sci.*, 2019, **10**, 10749-10754.
16. Z. J. Barton, J. Hui, N. B. Schorr and J. Rodríguez-López, *Electrochim. Acta*, 2017, **241**, 98-105.
17. T. Yamanaka, H. Nakagawa, S. Tsubouchi, Y. Domi, T. Doi, T. Abe and Z. Ogumi, *ChemSusChem*, 2017, **10**, 855-861.
18. Z. J. Barton and J. Rodríguez-López, *Anal. Chem.*, 2014, **86**, 10660-10667.
19. J. Hui, M. Burgess, J. Zhang and J. Rodríguez-López, *ACS Nano*, 2016, **10**, 4248-4257.
20. E. Ventosa and W. Schuhmann, *Phys. Chem. Chem. Phys.*, 2015, **17**, 28441-28450.
21. P. K. Hansma, B. Drake, O. Marti, S. A. C. Gould and C. B. Prater, *Science*, 1989, **243**, 641-643.
22. C.-C. Chen, Y. Zhou and L. A. Baker, *Annu. Rev. Anal. Chem.*, 2012, **5**, 207-228.
23. A. Page, D. Perry and P. R. Unwin, *Proc. R. Soc. A*, 2017, **473**, 20160889.
24. N. Ebejer, M. Schnippering, A. W. Colburn, M. A. Edwards and P. R. Unwin, *Anal. Chem.*, 2010, **82**, 9141-9145.
25. M. E. Snowden, A. G. Güell, S. C. S. Lai, K. McKelvey, N. Ebejer, M. A. O'Connell, A. W. Colburn and P. R. Unwin, *Anal. Chem.*, 2012, **84**, 2483-2491.
26. L. Danis, S. M. Gateman, C. Kuss, S. B. Schougaard and J. Mauzeroll, *ChemElectroChem*, 2017, **4**, 6-19.

27. P. Schwager, H. Bülter, I. Plettenberg and G. Wittstock, *Energy Technol.*, 2016, **4**, 1472-1485.
28. Z. J. Barton and J. Rodríguez-López, *Anal. Chem.*, 2017, **89**, 2716-2723.
29. M. A. Claudio-Cintrón and J. Rodríguez-López, *Anal. Chim. Acta*, 2019, **1069**, 36-46.
30. Z. J. Barton and J. Rodríguez-López, *Anal. Chem.*, 2017, **89**, 2708-2715.
31. R. M. Souto, Y. González ‐ García, D. Battistel and S. Daniele, *Chem. Eur. J.*, 2012, **18**, 230-236.
32. M. Tang and J. Newman, *J. Electrochem. Soc.*, 2011, **158**, A530-A536.
33. O. C. Harris and M. H. Tang, *J. Phys. Chem. C*, 2018, **122**, 20632-20641.
34. K. Hernández-Burgos, Z. J. Barton and J. Rodríguez-López, *Chem. Mater.*, 2017, **29**, 8918-8931.
35. J. Hui, N. B. Schorr, S. Pakhira, Z. Qu, J. L. Mendoza-Cortes and J. Rodríguez-López, *J. Am. Chem. Soc.*, 2018, **140**, 13599-13603.
36. S. Petnikota, N. K. Rotte, V. V. S. S. Srikanth, B. S. R. Kota, M. V. Reddy, K. P. Loh and B. V. R. Chowdari, *J. Solid State Electrochem.*, 2014, **18**, 941-949.
37. A. J. Bard, F. R. F. Fan, J. Kwak and O. Lev, *Anal. Chem.*, 1989, **61**, 132-138.
38. C. Tan, J. Rodríguez-López, J. J. Parks, N. L. Ritzert, D. C. Ralph and H. D. Abruña, *ACS Nano*, 2012, **6**, 3070-3079.
39. A. J. Bard and M. V. Mirkin, *Scanning electrochemical microscopy*, CRC Press, 2012.
40. P. Verma, P. Maire and P. Novák, *Electrochim. Acta*, 2010, **55**, 6332-6341.
41. B. H. Simpson and J. Rodríguez-López, *Electrochim. Acta*, 2015, **179**, 74-83.
42. K. Eckhard, X. Chen, F. Turcu and W. Schuhmann, *Phys. Chem. Chem. Phys.*, 2006, **8**, 5359-5365.
43. R. Cornut and C. Lefrou, *J. Electroanal. Chem.*, 2007, **608**, 59-66.
44. C. Lefrou, *J. Electroanal. Chem.*, 2006, **592**, 103-112.
45. C. G. Zoski, *Curr. Opin. Electrochem.*, 2017, **1**, 46-52.
46. Y. Li, Q. An, Y. Cheng, Y. Liang, Y. Ren, C.-J. Sun, H. Dong, Z. Tang, G. Li and Y. Yao, *Nano Energy*, 2017, **34**, 188-194.
47. C. Yang, J. Chen, T. Qing, X. Fan, W. Sun, A. von Cresce, M. S. Ding, O. Borodin, J. Vatamanu and M. A. Schroeder, *Joule*, 2017, **1**, 122-132.
48. X. Fan, L. Chen, O. Borodin, X. Ji, J. Chen, S. Hou, T. Deng, J. Zheng, C. Yang and S.-C. Liou, *Nat. Nanotechnol.*, 2018, **13**, 715.

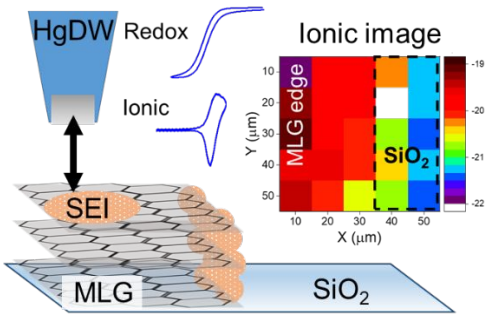

Mapping correlated ion and electron transfer reactivity as a passivating battery interphase evolves.